Research Article Vol. 4, No. 11 / November 2017 / Optica 1344

Efficient picosecond x-ray pulse generation from plasmas in the radiation dominated regime

Reed Hollinger,[1,6] Clayton Bargsten,[1] Vyacheslav N. Shlyaptsev,[1] Vural Kaymak,[4] Alexander Pukhov,[4] Maria Gabriela Capeluto,[5] Shoujun Wang,[1] Alex Rockwood,[2] Yong Wang,[1] Amanda Townsend,[2] Amy Prieto,[3] Patrick Stockton,[1] Alden Curtis,[1] and Jorge J. Rocca[1,2,*]

[1]Electrical and Computer Engineering Department, Colorado State University, Fort Collins, Colorado 80523, USA
[2]Physics Department, Colorado State University, Fort Collins, Colorado 80523, USA
[3]Chemistry Department, Colorado State University, Fort Collins, Colorado 80523, USA
[4]Institut für Theoretische Physik 1, Heinrich-Heine-Universität Düsseldorf, 40225 Düsseldorf, Germany
[5]Departamento de Física, FCEyN, UBA and IFIBA, CONICET, Pabellón 1, Ciudad Universitaria, 1428 Buenos Aires, Argentina
[6]e-mail: reed.hollinger@colostate.edu
*Corresponding author: jorge.rocca@colostate.edu

Received 24 July 2017; revised 29 September 2017; accepted 2 October 2017 (Doc. ID 303129); published 27 October 2017

The efficient conversion of optical laser light into bright ultrafast x-ray pulses in laser created plasmas is of high interest for dense plasma physics studies, material science, and other fields. However, the rapid hydrodynamic expansion that cools hot plasmas has limited the x-ray conversion efficiency (CE) to 1% or less. Here we demonstrate more than one order of magnitude increase in picosecond x-ray CE by tailoring near solid density plasmas to achieve a large radiative to hydrodynamic energy loss rate ratio, leading into a radiation loss dominated plasma regime. A record 20% CE into $h\nu > 1$ keV photons was measured in arrays of large aspect ratio Au nanowires heated to keV temperatures with ultrahigh contrast femtosecond laser pulses of relativistic intensity. The potential of these bright ultrafast x-ray point sources for table-top imaging is illustrated with single shot flash radiographs obtained using low laser pulse energy. These results will enable the deployment of brighter laser driven x-ray sources at both compact and large laser facilities.

OCIS codes: (040.7480) X-rays, soft x-rays, extreme ultraviolet (EUV); (320.7090) Ultrafast lasers; (110.7440) X-ray imaging; (350.5400) Plasmas; (160.4236) Nanomaterials.

https://doi.org/10.1364/OPTICA.4.001344

1. INTRODUCTION

Intense ultrashort bursts of x-ray radiation are essential for backlighting the implosion of capsules in inertial confinement fusion experiments [1,2]. They are also of significant interest for fundamental studies that include laboratory opacity measurements in matter at the conditions of stellar interiors [3], and for probing ultrafast changes in material with high spatial and temporal resolution [4,5]. Dense plasmas produced by laser irradiation of solid density materials with intense femtosecond laser pulses are emitters of intense x-ray pulses. However, different factors contribute to limit the CE into ultrafast x-ray pulses. First, only a fraction of the laser energy is absorbed by the plasma. Second, the radiation typically originates from a shallow plasma volume whose rapid expansion results in hydrodynamic cooling rates that exceed the radiation cooling rate. The result is poor conversion efficiency. Efforts to increase the ultrafast x-ray yield have largely focused on addressing the first of these two limitations by improving the coupling of the laser energy into the material using structured targets. Targets investigated include micro-lithographic gratings [6–8], nanometer-size dielectric spheres or ellipsoids [9,10], "smoked" clustered surfaces [7,11,12], and nanowire arrays [12–16]. Increased CE with respect to flat solid targets has been reported [6,11,12,14–17]. In the case of nanowires, the increased x-ray yield was often adjudicated to increased absorption [12,14], including enhanced absorption due to a "lightning rod effect" that increases the number of hot electrons as a result of an enhancement of the electric field at the tip of nanostructures [15,17]. In addition to increased absorption, Kulcsar *et al.* suggested other causes that include a larger number of heated atoms [12]. However, the CE into $h\nu > 0.9$ keV x-rays was limited to ~0.1%, a value similar to that obtained using smoke targets. In all the experiments with different types of nanostructured targets, the x-ray CE into $h\nu > 1$ keV photons has remained less than 1%, in spite of the increase in energy coupling. This CE into picosecond x-ray pulses is significantly lower than that achieved in converting laser light into nanosecond x-ray pulses in underdense gas or cavity and pre-exploded foil plasmas [18–22].

In this paper, we show that an increase of more than one order of magnitude in optical to picosecond x-ray CE can be achieved by tailoring the plasma characteristics to reach a smaller radiative

cooling time, τ_{rad}, than the hydrodynamic cooling time, τ_{hydro}, resulting in a larger radiative to hydrodynamic cooling rate ratio that effectively overcomes hydrodynamic cooling. The radiative cooling time is defined here as the time needed to radiatively dissipate the thermal energy of the plasma. In the simple case of an ideal plasma with ions of average charge Z, this characteristic time can be expressed as the ratio of the kinetic energy of free electrons to their rate of radiated energy loss by collisions: $\frac{3ZkT_e}{2E}\frac{1}{\langle\sigma v\rangle n_e}$, where σ is the effective electron collision cross section for all three major radiative processes (line radiation, photorecombination, and bremsstrahlung), T_e and n_e are the electron temperature and density, respectively, and E is the average energy radiated per collision event. The hydrodynamic cooling time is defined here as $\Delta L/C_s$, where ΔL is plasma size and C_s is the acoustic velocity. Considering that, within the range of high electron densities and high temperatures of interest for x-ray generation, τ_{rad} is inversely proportional to the electron-density-dependent total collision rate $\langle\sigma v\rangle n_e$ and τ_{hydro} is proportional to the plasma size ΔL, this condition requires a large electron density and/or large plasma size such that

$$\tau_{\mathrm{rad}} \propto \frac{1}{\langle\sigma v\rangle n_e} < \frac{\Delta L}{C_s} \propto \tau_{\mathrm{hydro}}. \quad (1)$$

We experimentally demonstrate that this approach results in an ~20% CE of optical laser light into $h\nu > 1$ keV x-rays in 4π sr, more than one order of magnitude increase in CE with respect to previous work. We fulfilled the inequality in Eq. (1) by volumetrically heating supercritical density plasmas by irradiating arrays of high aspect ratio Au or Ni nanowires at an intensity of $I \sim 4 \times 10^{19}$ W cm^{-2} with ultrahigh contrast femtosecond laser pulses. The interaction was tailored to simultaneously achieve deep volumetric heating (large ΔL) to multi-keV temperatures, and plasma densities of the order of 100 times the critical density in which the collisional rates are greatly increased with respect to plasmas generated from solid targets.

2. METHODS

The experiments were conducted by irradiating arrays of free-standing, vertically aligned Au and Ni nanowires with diameters of 55, 80, or 100 nm and 4–6 μm in length. The laser beam impinged parallel to the nanowire axis, normal to the nanowire array target surface. The nanowire arrays were synthesized by electrodeposition into anodic aluminum oxide templates [23]. The nanowires were grown with an average density of 12% solid density for the targets composed of 55 or 80 nm diameter nanowires, and 15% of solid density for the 100 nm diameter nanowire targets. After dissolving the template, an array of ordered, high aspect ratio (~50–100∶1) nanowires is exposed. This corresponds to an interwire spacing of 85 and 130 nm for the 55 and 100 nm diameter wire arrays, respectively. Each nanowire target was imaged using a scanning electron microscope. The nanostructured targets were irradiated by ultrahigh ($>10^{12}$) contrast $\lambda = 400$ nm pulses of ~55 fs duration with energy up to 1 J from a frequency-doubled Ti:sapphire chirped-pulse-amplification (CPA) laser. The laser consists of a conventional front end followed by three Ti:sapphire power amplifiers pumped by Nd:glass slab lasers designed to operate at up to 5 Hz repetition rate [24]. The beam was expanded to 9 cm, and the pulses were compressed using a gold grating vacuum compressor. Frequency doubling in a 0.8 mm thick Type I KDP crystal with an efficiency of 40%–50% greatly improves the contrast, as the second-harmonic generation process is proportional to the square of the intensity. The duration of the frequency-doubled pulse was measured in a single shot self-diffraction autocorrelator. The wavefront was corrected with a deformable mirror (Imagine Optic). The high contrast pulses were focused onto the target by a 90 deg off-axis parabolic mirror with a 15.4 cm focal length, resulting in a spot size of ~4.5 μm to obtain an intensity of $\sim 4 \times 10^{19}$ W cm^{-2}.

The angular distribution of the x-ray emission was measured using an array of four filtered Si photodiodes mounted at equally spaced polar angles on a 28 cm radius circular rail centered on the laser beam focus where the target was placed. Polished Ni or Au flat solid targets were shot immediately preceding each nanowire target shot for comparison. The diodes were placed on a plane that forms an angle of 20 deg with respect to the plane of incidence. Magnet pairs were placed in the front of each of the photodiodes to deflect electrons up to 6 MeV energy away from the diodes. It was verified that increasing the magnetic field strength by 2 × and the length of the magnets by the same factor did not change the photodiode signals, ensuring that the photodiode/filter assembly is in practice only detecting x-rays. The spectrally resolved x-ray emission was simultaneously recorded using a von Hamos mica crystal spectrometer and a front illuminated CCD. Time integrated spectral emission of the plasmas showed He-like Ni ion lines that dominate over the characteristic K-α emission by over one order of magnitude.

3. RESULTS AND DISCUSSION

Figure 1 illustrates a particle-in-cell simulation (PIC) of the electron temperature and electron density evolution in an array of Au nanowires at three different times after the laser pulse. The array is composed of wires 55 nm in diameter with an average density corresponding to 12% of solid density, and the laser pulse has a 55 fs FWHM duration. The simulation was conducted using the fully relativistic 3-D PIC code Virtual Laser-Plasma Laboratory (VLPL) [25]. In contrast to flat solid targets, where a thin plasma layer is heated, in nanowire arrays the ultrafast laser pulses propagate several micrometers within the interwire gaps. The heated nanowires explode, creating a thick plasma layer of nearly solid density, reaching $n_e \sim 4 \times 10^{23}$ cm^{-3} 311 fs after the peak of the laser pulse, while the electron temperature is ~15 keV [Figs. 1(c) and 1(f)]. Later the plasma cools, but 1 ps after the peak of the laser pulse the temperature still remains at a few keV. To illustrate the major radiative differences between a flat solid target and a volumetrically heated nanowire array, Fig. 2 shows the computed x-ray radiation power density spatial distribution as a function of time up to 10 ps after the laser pulse. The simulations are the result of hydrodynamic model computations with transient atomic kinetics in which the VLPL PIC code was used to simulate the first stages of nanowire plasma formation until the nanowires are fully dissolved. Both targets are assumed to be irradiated with an intensity of 4×10^{19} W cm^{-2}. It is shown that irradiation of the Au nanowire array results in both a large increase in the radiating volume and a larger emitted power density. In the case of the flat solid target, most of the x-ray emission takes place in a very thin supercritical layer heated by conduction, where acceleration and expansion cooling take place, with the plasma density rapidly dropping orders of magnitude in

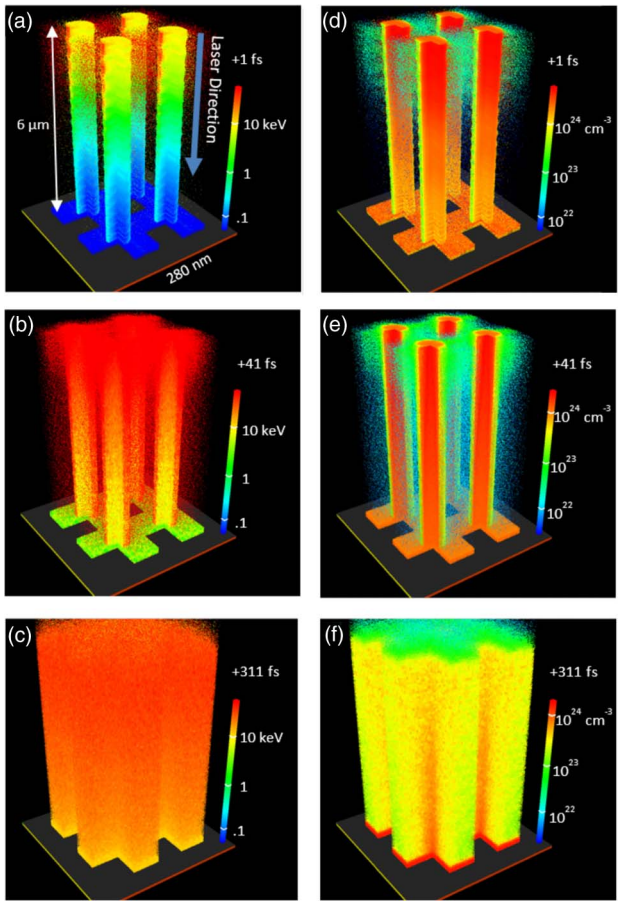

Fig. 1. (a)–(c) PIC simulation of the electron temperature distribution in a 55 nm diameter Au nanowire array irradiated by a $\lambda = 400$ nm laser pulse of 55 fs duration at an intensity of 4×10^{19} W cm^{-2} at three different times after the laser pulse. (d)–(f) show the corresponding electron density maps.

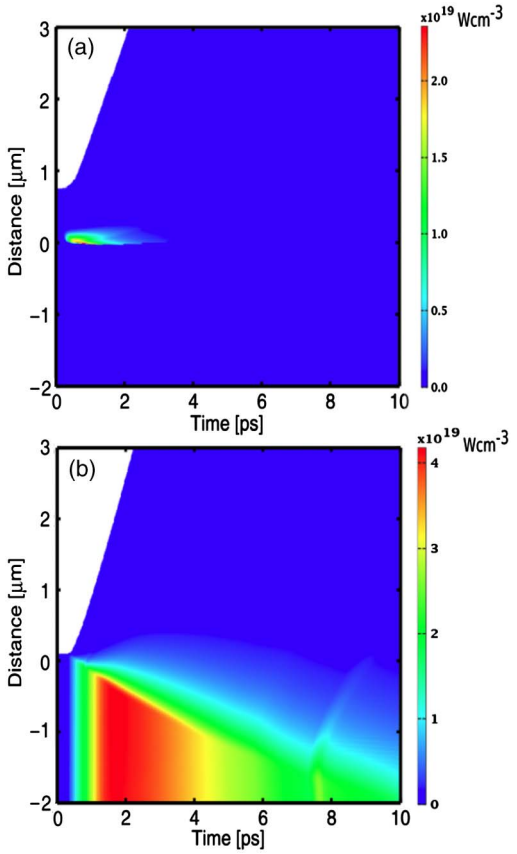

Fig. 2. Computed evolution of the x-ray radiation power for (a) a Au flat target and (b) a Au nanowire target, both irradiated at an intensity of 4×10^{19} W cm^{-2} with a 55 fs FWHM pulse. The array of nanowires is assumed to be composed of 55 nm diameter wires with an average density of 12% solid. Time is measured with respect to the peak of the laser pulse, and the distance is in the direction normal to the target surface.

1 mm. The much larger heated plasma depth in the nanowire plasma greatly increases the plasma hydrodynamic cooling time. Simultaneously, the larger plasma density results in an increased electron collisional excitation rate, leading to a shorter radiative cooling time.

The magnitude of these effects is quantitatively illustrated in Fig. 3 by atomic kinetic calculations that compare the characteristic radiative and hydrodynamic cooling times of a Au flat target plasma and a Au nanowire array plasma. The computations were conducted with the hydrodynamic/atomic physics code Radex [26]. Figure 3(a) shows the cooling times for Au plasma with a density of $n_e = 6 \times 10^{22}$ cm^{-3} and a thickness of 0.2 μm. These are the typical parameters of the x-ray emitting layer computed by both PIC and hydrodynamic models for plasmas created by irradiating a solid Au target. Both models give similar source thickness values in spite of the fact that RADEX is approaching the validity limit of the hydrodynamic approximation. In this case, the great majority of the laser energy is lost in the hydrodynamic expansion before collisions have time to convert the electron kinetic energy into radiation. For the electron temperatures of interest, the hydrodynamic cooling time is much shorter than the radiative cooling time, resulting in a small CE. This result is in contrast to Fig. 3(b) for a supercritical Au plasma with a density of $n_e = 4 \times 10^{23}$ cm^{-3}, a value approaching 100 times the critical density, typical of the conditions resulting from irradiating the nanowire arrays with the intensity we used in the experiments. In this case the radiative cooling time is smaller than the hydrodynamic cooling time, leading to greatly increased radiation efficiency.

For larger average density nanowire arrays irradiated at increased intensities, even higher electron densities will result [27], further driving the plasma into a radiation loss dominated regime.

The large increase in CE we report here is made possible by selecting a combination of irradiation and target parameters designed to achieve the condition in Eq. (1). First, we use ultrahigh contrast $>10^{12}$ laser pulses that avoid destroying the nanowires and establishing a critical density layer before the main pulse arrives. Second, we use short laser pulses (55 fs) that allow for nearly all of the laser energy to be deposited deep into the array before the nanowires explode and close the interwire gap, forming a continuous critical density surface. After this time, no further efficient coupling of the laser energy can occur into the volumetrically heated plasma. Third, the use of long nanowires allows for volumetric heating to occur to depths of 4–5 μm [27], increasing the hydrodynamic expansion time. Fourth, we use dense arrays, in which the plasma density reaches nearly 100 times the critical

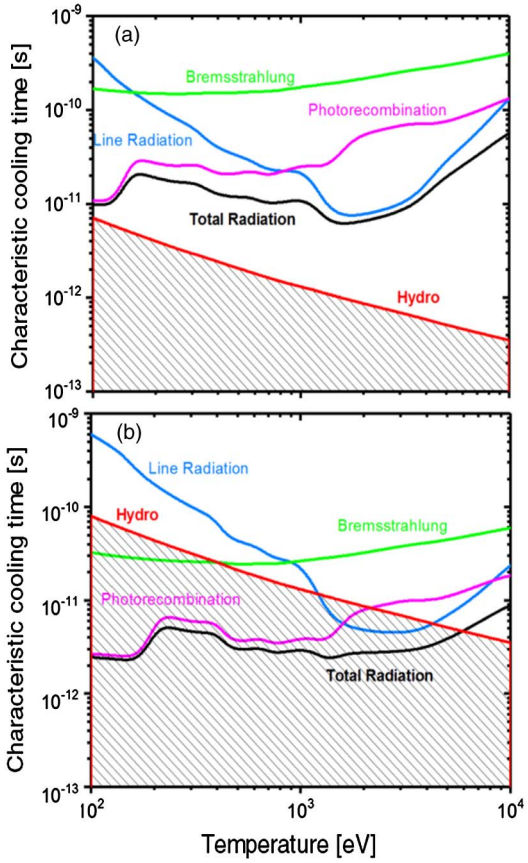

Fig. 3. Comparison of radiative and hydrodynamic cooling times as a function of electron temperature for two different Au plasmas with characteristics corresponding to the x-ray emitting region of (a) a flat solid target, $n_e = 6 \times 10^{22}$ cm^{-3}, plasma size $L = 0.2$ μm, and (b) a nanowire array plasma $n_e = 4 \times 10^{23}$ cm^{-3} and plasma size $L = 4$ μm. The total radiation time is the effective radiative cooling time computed from the photorecombination, bremsstrahlung, and line radiation rates.

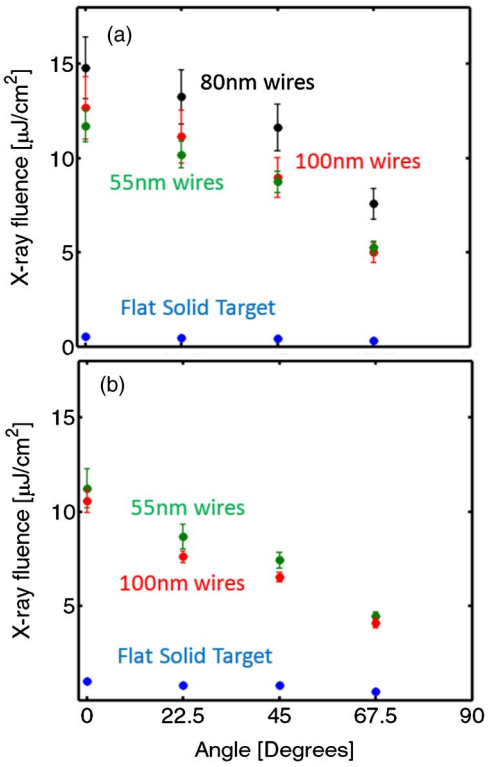

Fig. 4. Measured angular distribution of the x-ray fluence on each diode from nanowire arrays at photon energies >1 keV for (a) Au and (b) Ni nanowire targets of different nanowire diameters. Measurements for flat solid targets of the same materials are included for comparison. The irradiation intensity was 4×10^{19} W cm^{-2}. Error bars correspond to 1 standard deviation. Fluctuations in x-ray CE result mostly from irregularities and imperfections in the ordered wire array. The angle is measured with respect to the normal to the target surface.

density, which results in high collisional rates and, consequently, in very short radiative cooling times. Fifth, we use relativistic irradiation intensities that heat the plasmas to multi-keV temperatures deep into the array, which leads to a high degree of ionization [16], an increased electron density, and a decreased radiation lifetime. This simultaneous set of conditions differs from those in previous experiments that measured x-ray yield from nanowire targets. Prior work used either picosecond pulses [12], short wires [12,14], relatively low contrast pulses [12–14], or non-relativistic intensities [11–14]. This limited the radiation fraction obtained for $h\nu > 1$ keV to values nearly two orders of magnitude smaller than that we report here.

For photon energies $h\nu > 1$ keV, both Au and Ni nanowires display a convex angular emission profile with maximum intensity in the direction normal to the target (Fig. 4), resulting from increased opacity in the periphery of the plasma. Integration of these emission profiles over a hemisphere gives us the total x-ray yields shown in Fig. 5. Comparison of the x-ray CE for Au and Ni nanowire array targets of different wire diameters shows that the x-ray emission is higher for Au. CE is defined here as the ratio of the measured x-ray energy for photons $h\nu > 1$ keV (or >6 keV) emitted into 4π sr divided by the laser drive energy impinging onto the target. The highest yield corresponds to targets with 80 nm diameter Au nanowires, with an average CE of 18% and individual shots reaching values up to 22% in 4π sr [Fig. 5(a)]. This CE for $h\nu > 1$ keV exceeds the highest reported values reported using any type of target by more than one order of magnitude [6] and those reported for nanowire targets by two orders of magnitude [12]. Figure 5(b) compares the $h\nu > 6$ keV plasma emission from Au nanowire targets of different nanowire diameters to that from a Au foil target irradiated with the same pulses. At these energies, the active region of the Si detector starts to become transparent to the radiation. We corrected the measured photodiode signal for the 50 μm thickness of the Si detector active region, and also for the energy dependency of the filter transmissivity. For the latter, since model simulations show there is no line radiation above 6 keV for these transient Au plasmas, we assumed the spectral distribution is that resulting from bremsstrahlung plus photorecombination. This continuum radiation was calculated using the electron energy distribution computed by PIC simulations. With these corrections, the 80 nm Au nanowire targets are estimated to radiate at $h\nu > 6$ keV with a CE that exceed 0.8% in 4π sr, an increase of 14 times over Au foils irradiated by the same laser pulses.

The increase in x-ray flux, the small source size of ~5 μm deduced from the penumbra in a knife edge test, and the picosecond pulse duration makes these plasmas an excellent x-ray point source for time-resolved flash radiography. To illustrate this,

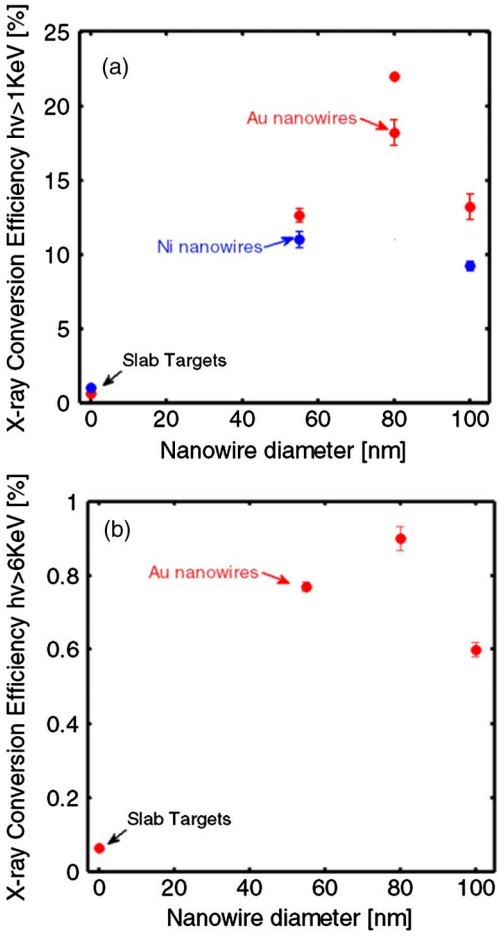

Fig. 5. (a) x-ray CE ($h\nu > 1$ keV) for Au and Ni nanowire arrays of different wire diameters compared to flat solid targets of the same material. $I = 4 \times 10^{19}$ W cm^{-2}. The values are averages of 10 shots. Error bars correspond to 1 standard deviation. The maximum measured single shot CE for 80 nm diameter wires exceeded 22% in 4π sr, which is represented by the point without an error bar. This yield corresponds to an increase of 35 × with respect to a polished flat target; (b) CE into $h\nu > 6$ keV x-rays. An enhancement of 14 × in x-ray emission is observed compared to flat targets.

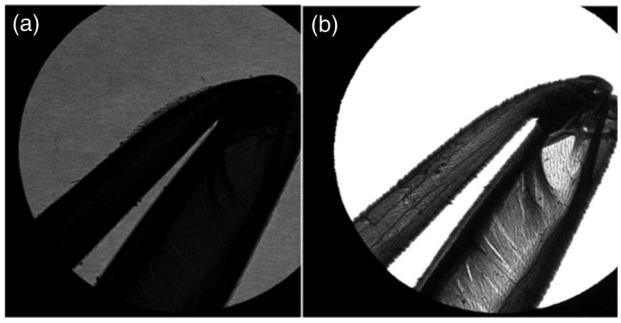

Fig. 6. Single shot radiograph of a wasp's knee using the x-ray flash emitted from (a) a flat Ni target, and (b) an array of 100 nm Ni nanowires. A 13 μm Be filter was used to block photons of $h\nu < 1$ keV. The sample was placed at 4 cm from the plasma, and a CCD array was placed at a distance of 35 cm from the sample, leading to an effective magnification of 8.75 × with a field of view of 425 μm. Both images are plotted on the same intensity scale. The laser energy on target was 25 mJ.

we conducted a single shot radiography experiment of a wasp's knee. Figure 6(b) compares a single shot radiograph taken by irradiating an array of 100 nm diameter Ni nanowires with 15% solid density to that obtained by irradiating a flat Ni solid target with a similar laser pulse [Fig. 6(a)]. The radiograph taken with the nanowire target shows that a single laser shot with a laser pulse energy of only 25 mJ on target is sufficient to produce a detailed image. In comparison, the image obtained with the flat Ni target shows insufficient flux and would require over one order of magnitude more shots to obtain a similar image.

4. CONCLUSIONS

In conclusion, we have demonstrated that the CE of optical laser pulses into picosecond x-ray pulses can be greatly improved by increasing the radiative to hydrodynamic energy loss rate ratio in volumetrically heated supercritical density plasmas. By tailoring nanostructured targets irradiated at relativistic intensities to fulfill this condition, we have generated ultrafast pulses of $h\nu > 1$ keV photons with a record efficiency of ~20% into 4π sr. This increase of more than one order of magnitude in the efficient generation of picosecond line and continuum x-ray radiation will open new opportunities in flash radiography, including the backlighting of imploding capsules in laser fusion experiments, in opacity measurements of matter at the conditions of stellar interiors, and in table-top applications requiring intense picosecond flashes of x-rays. Furthermore, the results will also motivate more efficient x-ray generation experiments at larger laser facilities.

Funding. Fusion Sciences Program of the Office of Science (SC) of the U.S. Department of Energy (DE-SC0014610)

Acknowledgment. We acknowledge encouraging discussions with Michael Purvis and the use of the CU-CSU Summit Computer (ACI-1532235) and previous support from the Defense Threat Reduction Agency (HDTRA-1-10-1-0079).

REFERENCES

1. F. J. Marshall, P. W. McKenty, J. A. Delettrez, R. Epstein, J. P. Knauer, V. A. Smalyuk, J. A. Frenje, C. K. Li, R. D. Petrasso, F. H. Séguin, and R. C. Mancini, "Plasma-density determination from x-ray radiography of laser-driven spherical implosions," Phys. Rev. Lett. **102**, 185004 (2009).
2. C. M. Huntington, C. M. Krauland, C. C. Kuranz, R. P. Drake, H. S. Park, D. H. Kalantar, B. R. Maddox, B. A. Remington, and J. Kline, "Development of a short duration backlit pinhole for radiography on the National Ignition Facility," Rev. Sci. Instrum. **81**, 10E536 (2010).
3. J. E. Bailey, T. Nagayama, G. P. Loisel, G. A. Rochau, C. Blancard, J. Colgan, P. Cosse, G. Faussurier, C. J. Fontes, F. Gilleron, I. Golovkin, S. B. Hansen, C. A. Iglesias, D. P. Kilcrease, J. J. Macfarlane, R. C. Mancini, S. N. Nahar, C. Orban, J. Pain, A. K. Pradhan, M. Sherrill, and B. G. Wilson, "A higher-than-predicted measurement of iron opacity at solar interior temperatures," Nature **517**, 56–59 (2015).
4. B. Yaakobi, T. R. Boehly, D. D. Meyerhofer, T. J. B. Collins, B. A. Remington, P. G. Allen, S. M. Pollaine, H. E. Lorenzana, and J. H. Eggert, "EXAFS measurement of iron bcc-to-hcp phase transformation in nanosecond-laser shocks," Phys. Rev. Lett. **95**, 1–4 (2005).
5. A. Cavalleri, C. W. Siders, F. L. H. Brown, D. M. Leitner, C. Tóth, J. A. Squier, C. P. J. Barty, K. R. Wilson, K. Sokolowski-Tinten, M. Horn Von Hoegen, D. von Der Linde, and M. Kammler, "Anharmonic lattice dynamics in germanium measured with ultrafast x-ray diffraction," Phys. Rev. Lett. **85**, 586–589 (2000).
6. M. M. Murnane, H. C. Kapteyn, S. P. Gordon, J. Bokor, E. N. Glytsis, and R. W. Falcone, "Efficient coupling of high-intensity subpicosecond laser pulses into solids," Appl. Phys. Lett. **62**, 1068–1070 (1993).

7. S. P. Gordon, T. Donnelly, A. Sullivan, H. Hamster, and R. W. Falcone, "X rays from microstructured targets heated by femtosecond lasers," Opt. Lett. **19**, 484–486 (1994).
8. S. Kahaly, S. K. Yadav, W. M. Wang, S. Sengupta, Z. M. Sheng, A. Das, P. K. Kaw, and G. R. Kumar, "Near-complete absorption of intense, ultrashort laser light by sub- gratings," Phys. Rev. Lett. **101**, 145001 (2008).
9. P. P. Rajeev, P. Taneja, P. Ayyub, A. S. Sandhu, and G. R. Kumar, "Metal nanoplasmas as bright sources of hard x-ray pulses," Phys. Rev. Lett. **90**, 115002 (2003).
10. H. A. Sumeruk, S. Kneip, D. R. Symes, I. V. Churina, A. V. Belolipetski, T. D. Donnelly, and T. Ditmire, "Control of strong-laser-field coupling to electrons in solid targets with wavelength-scale spheres," Phys. Rev. Lett. **98**, 45001 (2007).
11. F. Y. Khattak, R. J. Clarke, E. J. Divall, M. Edwards, P. S. Foster, C. J. Hooker, A. J. Langley, O. A. M. B. du Sert Percie, C. Spindloe, G. Tallents, D. Riley, P. Mistry, D. Neely, J. Smith, and M. Tolley, "Enhanced He-alpha emission from "smoked" Ti targets irradiated with 400 nm, 45 fs laser pulses," Europhys. Lett. **72**, 242–248 (2005).
12. G. Kulcsar, D. AlMawlawi, F. Budnik, P. Herman, M. Moskovits, L. Zhao, and R. Marjoribanks, "Intense picosecond x-ray pulses from laser plasmas by use of nanostructured 'Velvet' targets," Phys. Rev. Lett. **84**, 5149–5152 (2000).
13. T. Nishikawa, H. Nakano, K. Oguri, N. Uesugi, M. Nakao, K. Nishio, and H. Masuda, "Nanocylinder-array structure greatly increases the soft x-ray intensity generated from femtosecond-laser-produced plasma," Appl. Phys. B **73**, 185–188 (2001).
14. A. V. Ovchinnikov, O. F. Kostenko, O. V. Chefonov, O. N. Rosmej, N. E. Andreev, M. B. Agranat, J. L. Duan, J. Liu, and V. E. Fortov, "Characteristic x-rays generation under the action of femtosecond laser pulses on nano-structured targets," Laser Part. Beams **29**, 249–254 (2011).
15. S. Mondal, I. Chakraborty, S. Ahmad, D. Carvalho, P. Singh, A. D. Lad, V. Narayanan, P. Ayyub, G. R. Kumar, J. Zheng, and Z. M. Sheng, "Highly enhanced hard x-ray emission from oriented metal nanorod arrays excited by intense femtosecond laser pulses," Phys. Rev. B **83**, 1–5 (2011).
16. M. A. Purvis, V. N. Shlyaptsev, R. Hollinger, C. Bargsten, A. Pukhov, A. Prieto, Y. Wang, B. M. Luther, L. Yin, S. Wang, and J. J. Rocca, "Relativistic plasma nanophotonics for ultrahigh energy density physics," Nat. Photonics **7**, 796–800 (2013).
17. P. P. Rajeev, P. Ayyub, S. Bagchi, and G. R. Kumar, "Nanostructures, local fields, and enhanced absorption in intense light-matter interaction," Opt. Lett. **29**, 2662–2664 (2004).
18. M. J. May, Y. P. Opachich, G. E. Kemp, J. D. Colvin, M. A. Barrios, K. W. Widmann, K. B. Fournier, M. Hohenberger, F. Albert, and S. P. Regan, "Demonstration of a long pulse x-ray source at the National Ignition Facility," Phys. Plasmas **24**, 042701 (2017).
19. F. Pérez, J. J. Kay, J. R. Patterson, J. Kane, B. Villette, F. Girard, C. Reverdin, M. May, J. Emig, C. Sorce, J. Colvin, S. Gammon, J. Jaquez, J. H. Satcher, and K. B. Fournier, "Efficient laser-induced 6–8 keV x-ray production from iron oxide aerogel and foil-lined cavity targets," Phys. Plasmas **19**, 083101 (2012).
20. E. L. Dewald, M. Rosen, S. H. Glenzer, L. J. Suter, F. Girard, J. P. Jadaud, J. Schein, C. Constantin, F. Wagon, G. Huser, P. Neumayer, and O. L. Landen, "X-ray conversion efficiency of high-Z Hohlraum wall materials for indirect drive ignition," Phys. Plasmas **15**, 072706 (2008).
21. D. Babonneau, M. Primout, F. Girard, J. P. Jadaud, M. Naudy, B. Villette, S. Depierreux, C. Blancard, G. Faussurier, K. B. Fournier, L. Suter, R. Kauffman, S. Glenzer, M. C. Miller, J. Grün, and J. Davis, "Efficient multi-keV x-ray sources from laser-exploded metallic thin foils," Phys. Plasmas **15**, 092702 (2008).
22. C. A. Back, J. Grun, C. Decker, L. J. Suter, J. Davis, O. L. Landen, R. Wallace, W. W. Hsing, J. M. Laming, U. Feldman, M. C. Miller, and C. Wuest, "Efficient multi-keV underdense laser-produced plasma radiators," Phys. Rev. Lett. **87**, 275003 (2001).
23. A. L. Prieto, M. Martín-González, J. Keyani, R. Gronsky, T. Sands, and A. M. Stacy, "The electrodeposition of high-density, ordered arrays of $Bi_{1-x}Sb_x$ nanowires," J. Am. Chem. Soc. **125**, 2388–2389 (2003).
24. D. H. Martz, D. Alessi, B. M. Luther, Y. Wang, D. Kemp, M. Berrill, and J. J. Rocca, "High-energy 13.9 nm table-top soft-x-ray laser at 2.5 Hz repetition rate excited by a slab-pumped Ti:sapphire laser," Opt. Lett. **35**, 1632–1634 (2010).
25. A. Pukhov, "Three-dimensional electromagnetic relativistic particle-in-cell code VLPL (Virtual Laser Plasma Lab)," J. Plasma Phys. **61**, 425–433 (1999).
26. A. V. Vinogradov and V. N. Shlyaptsev, "Characteristics of a laser plasma x-ray source (review)," Sov. J. Quantum Electron. **17**, 1–14 (1987).
27. C. Bargsten, R. Hollinger, M. G. Capeluto, V. Kaymak, A. Pukhov, S. Wang, A. Rockwood, Y. Wang, D. Keiss, R. Tommasini, R. London, J. Park, M. Busquet, M. Klapisch, V. N. Shlyaptsev, and J. J. Rocca, "Energy penetration into arrays of aligned nanowires irradiated with relativistic intensities: scaling to terabar pressures," Sci. Adv. **3**, 3–11 (2017).